Iron Ore Sintering Process Model to Study Local Permeability Control

Y. Kaymak[1], T. Hauck[1], M. Hillers[2]
1. VDEh Betriebsforschungsinstitute GmbH, Düsseldorf, NW, Germany
2. Shuangliang Clyde Bergemann GmbH, Ratingen, NW, Germany

Introduction

The iron ore sintering process prepares the fine iron ores for the blast furnace process. Sinter plants agglomerate iron ore fines with other fine materials at high temperature in a mix bed to create a product that can be used in a blast furnace. Main feed into a sinter plant is base mix, which consists of iron ore fines, coke fines and flux (lime stone) fines and iron bearing residues. The base mix is ignited at the top and air is sucked from below to move the combustion front downwards through the bed while it moves as shown in Figure 1. The process causes the constituent materials to fuse, yielding a porous mass.

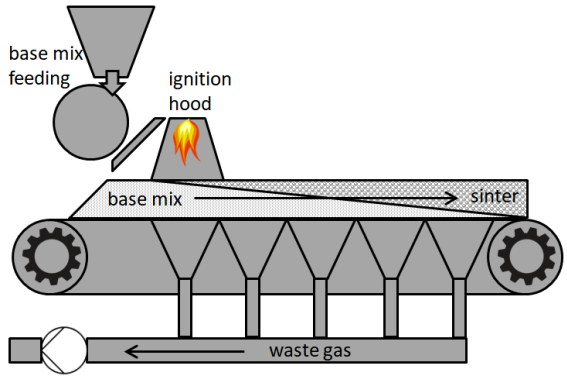

Figure 1. Sinter process scheme.

Benefit of this process is to allow recycling of residues from other sections of the plant, such as flue dust, mill scale, lime dust and sludge.

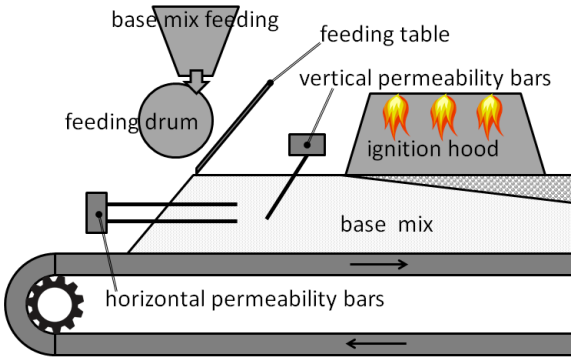

Figure 2. Typical placement configurations of the horizontal and vertical permeability bars in a sinter plant base mix feeding system.

The efficiency of the process can be improved by permeability bars, which locally increase the porosity of the bed. This improves the air supply to the coke combustion. The permeability bars can be arranged horizontally or vertically, as shown in Figure 2. A photo of horizontal permeability bars in action is also shown in Figure 3. These bars ultimately affect the local flow rates, the local course of the combustion, the temperature field in the bed and thus the overall sinter process characteristic. The influence on the bed temperature can directly be observed at the discharge position of the bed. A time averaged thermographic image for the two horizontal permeability bar configurations at discharge is shown in Figure 4.

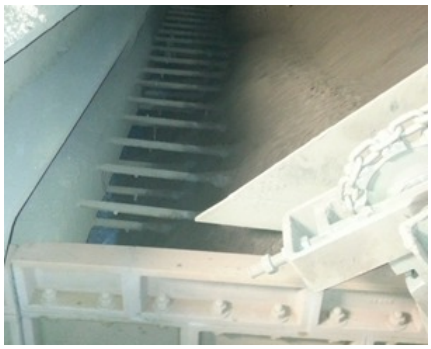

Figure 3. Sinter plant feeding system in operation with two rows of horizontal permeability bars.

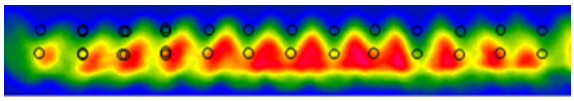

Figure 4. Time averaged thermography at discharge.

A transient 2D sinter process model was developed to investigate the influence of various permeability bar configurations on the process. This model solves the equations for reactions and flow through the porous bed with the Chemical Reaction Engineering Module in COMSOL Multiphysics®. The simulation model has been calibrated with plant and laboratory measurements and laboratory experiments. The temperature profiles for different permeability bar configurations are observed by IR-thermography at the plant discharge. Moreover, the local changes of the permeability were measured via air velocity measurements. The model results were proven to be consistent to the lab and plant measurements.

Theory and Governing Equations

The sinter process simulation model presented here solves the reacting flow through porous bed problem. It is essential for this study to model the influence of local permeability changes. In summary, the model includes all of the relevant sub-processes within the sintering process as listed below:

1. heat transfer in gas and solids
2. heat exchange between gas and solids,
3. melting and solidification enthalpies.
4. gas flow through the porous bed,
5. porosity sub-model,
6. mass exchange between gas and solids
7. transport of concentrated species in gas,
8. drying and condensation,
9. coke burn-out
10. calcination,
11. sulfation.

The governing PDEs for each of these sub-process models are described briefly as next.

Heat exchange between gas and solids:
The temperature field of the gas phase is modelled by the heat transfer in fluids physics:

$$\rho_g C_{pg} \frac{\partial T_g}{\partial t} + \rho_g C_{pg} \mathbf{u} \cdot \nabla T_g + \nabla \cdot \mathbf{q}_g = Q_g - Q_{gs}$$
$$\mathbf{q}_g = -k_g \nabla T_g$$

Similarly, the temperature field of the sinter bed is modelled by the heat transfer in solids physics:

$$\rho_s C_p \frac{\partial T_s}{\partial t} + \nabla \cdot \mathbf{q}_s = Q_s + Q_{gs}$$
$$\mathbf{q}_s = -k_s \nabla T_s$$

In these equations, subscript g is for gas and s is for sinter bed; ρ is the density, C_p heat capacity, T temperature, t time, $\mathbf{u}$ gas velocity vector, $\mathbf{q}$ heat flux vector, k heat conductivity, Q heat source term due to chemical reactions, Q_{gs} is the heat exchange between gas and solid. The equations for the heat exchange Q_{gs} depends on the temperature difference between gas and the solid as well as the heat transfer coefficient α, which are defined by:

$$Q_{gs} = \left(T_g - T_s\right) \cdot \frac{\alpha \cdot 6 \cdot (1-\varepsilon_s)}{d_s}$$
$$\alpha = \frac{k_g}{d_s}\left(2 + 0.6 \cdot Re^{0.5} \cdot Pr^{0.333}\right)$$

where, ε_s is local porosity of the sinter bed and d_s, the equivalent particle diameter for the heat exchange, k_g heat conductivity of the gas. Re and Pr are Reynold's and Prandtl numbers, respectively.

Solidification and melting enthalpy is implemented in the heat capacity of the sinter bed C_{ps}, which is defined as a piecewise cubic interpolation function with linear extrapolations. The melting starts at T_{melt}^{start} =1050°C and ends at T_{melt}^{end} =1250°C. The melting and re-solidification enthalpy sets a maximum temperature limit of the process for a given fuel (coke) rate. The sinter quality (strength) is directly related to the temperature and duration of the melting and re-solidification. The permeability bars strongly influence the sinter quality distribution via the induced local differences in flow and their consequences.

Gas flow through the porous bed:
The gas flow through the porous sinter bed is modelled by the Brinkman Equation:

$$\frac{\rho_g}{\varepsilon_s}\left(\frac{\partial \mathbf{u}}{\partial t} + (\mathbf{u} \cdot \nabla)\frac{\mathbf{u}}{\varepsilon_s}\right) = \nabla \cdot \left[-p\mathbf{I} + \frac{\mu}{\varepsilon_s}\left\{(\nabla \mathbf{u} + (\nabla \mathbf{u})^T) - \frac{2}{3}(\nabla \cdot \mathbf{u})\mathbf{I}\right\}\right] - \left(\boldsymbol{\kappa}^{-1}\mu + \beta_F|\mathbf{u}| + \frac{Q_{br}}{\varepsilon_s^2}\right)\mathbf{u}$$

where, ρ is the gas density, ε_s is porosity, $\mathbf{u}$ is velocity vector, t is time, p is pressure, μ is dynamic viscosity, $\mathbf{I}$ is identity matrix, $\boldsymbol{\kappa}$ is permeability, β_F is Forchheimer coefficient, and Q_{br} is mass source. The coefficients of the Brinkman equations are set such that it corresponds to the Ergun's equation:

$$\kappa = \frac{\varepsilon_s^3 \cdot d_s^2}{A_{Erg}(1-\varepsilon_s)^2 \cdot f_p f_{pbase}}$$
$$\beta_F = B_{Erg} \cdot \frac{(1-\varepsilon_s)}{\varepsilon_s^3 \cdot d_s \cdot \rho f_p f_{pbase}}$$

where, d_s means the equivalent diameter as in Ergun's equation, A_{Erg} coefficient of linear velocity term, B_{Erg} coefficient to quadratic velocity term, f_p is a factor for the change of porosity up on sintering shrinkage and $f_{pbase} = 3.5$ is a global calibration constant in Ergun's equation.

Porosity sub-model:
The local variation of the bed permeability and porosity is the main interest of this work in order to investigate the influence of the permeability bars on the sinter process. Therefore, the local variation of sinter bed porosity for horizontal and vertical permeability bars are determined by laboratory tests by measuring the air velocity directly above the mix bed. Similar to the sinter plant, the air is sucked from

below through the mix bed and the air velocities are measured at several grid positions. Figure 5 shows the grid at the top surface of the mix bed at the laboratory scale device. A set of measured air velocities is also shown in Figure 6, where different colors correspond to the height of measurement point above the bed and x-axis positions along A-G. By using these results, a porosity sub-model has been developed.

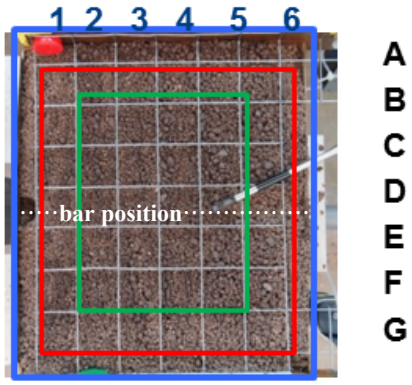

Figure 5. Air velocities measurements above the mix bed at laboratory.

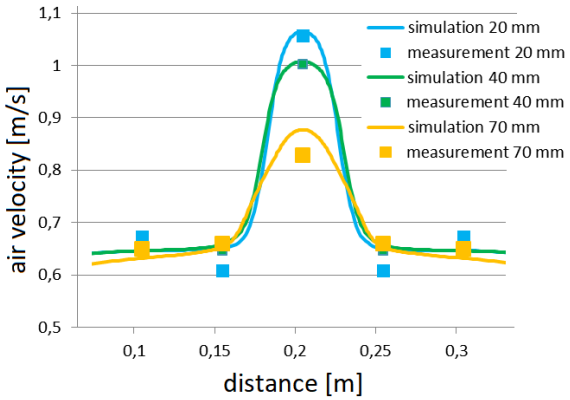

Figure 6. Measured air velocities above the mix bed and porosity model calibration.

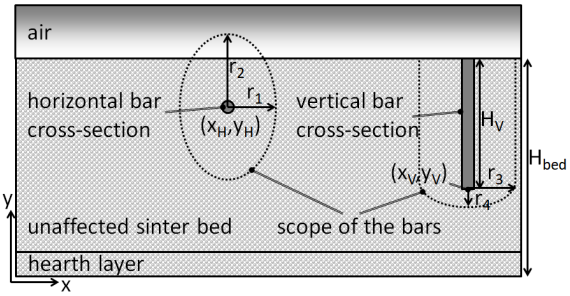

Figure 7. Porosity model.

Each permeability bar has its own scope which is an ellipse for horizontal bar and mostly rectangular for vertical bars. These scopes of improved aeration around the cross-section of the bars itself are shown in Figure 7. Beyond the scopes, the bed permeability is assumed to be unaffected. The main parameters of the porosity model (scope geometry, porosities) are calibrated by using the air velocity measurements (see Figure 6).

For example, a typical initial mix bed porosity is $\varepsilon_{s0} = 0.3$. The spatial distributions are modelled by distance functions and step functions. Distance (scope) functions for a horizontal bar $\hat{r}_H^2$ and vertical bar $\hat{r}_V^2$ are given as:

$$\hat{r}_H^2 = \frac{(x-x_H)^2}{r_1^2} + \frac{(y-y_H)^2}{r_2^2}$$

$$\hat{r}_V^2 = \begin{cases} \frac{(x-x_V)^2}{r_3^2} + \frac{(y-y_V)^2}{r_4^2} & \text{if } y < y_V \\ \frac{(x-x_V)^2}{r_3^2} & \text{otherwise} \end{cases}$$

where, $r_1 = r_3 \approx \sqrt{2} \cdot d_{H/V}$, $r_2 \approx \sqrt{5} \cdot d_{H/V}$ and $r_4 \approx d_{H/V}$. The diameter of horizontal or vertical bar is expressed by $d_{H/V}$. Then, the position dependent porosity can be simply expressed by:

$$\varepsilon_s(x,y) = \varepsilon_{s0} + \Delta\varepsilon \cdot \left(\text{step}(\hat{r}_H^2) + \text{step}(\hat{r}_V^2)\right)$$

The spatial porosity distribution in the mix bed for the horizontal and vertical permeability bars are quite well described with the above equation (see the porosity distributions in Figure 12 and Figure 16, note that in these figures the left and right vertical boundaries define symmetry planes of periodicity).

Transport of concentrated species:

The sinter process model involves chemical reactions. Therefore it is necessary to model the transport of the species in gas mix and species concentrations in sinter mix. For the gas, a mixture averaged convection model is used for the transport of concentrated species (namely, N2, O2, CO2, H2O, SO2). The mixture gas density is computed by the ideal gas law. The reaction rates are given by:

$$R_{wN2} = 0 \, \frac{kg}{m^3 \cdot s}$$

$$R_{wO2} = M_{O2} \cdot (-r_C N_C - 0.5 \cdot r_S N_L) \, \frac{kg}{m^3 \cdot s}$$

$$R_{wCO2} = M_{CO2} \cdot (-r_C N_C - r_{Ca} N_L) \, \frac{kg}{m^3 \cdot s}$$

$$R_{wH2O} = M_{H2O} \cdot (R_{H2O}) \, \frac{kg}{m^3 \cdot s}$$

$$R_{wSO2} = M_{SO2} \cdot (r_C N_C f_S^{coke} - r_S N_L) \, \frac{kg}{m^3 \cdot s}$$

where M is the molar mass of the species, f_S^{coke} is the fraction of sulfur in coke, N_C & N_L number of coke and lime particles per unit volume, r_C & r_{Ca} & r_S

molar reaction rates of coke burn-out, calcination and sulfatation. R_{H2O} is molar drying rate per unit volume, its negative value indicates condensation.

Chemical reactions (drying/condensation, coke burn-out, calcination and sulfation) including gas and solid phases are further described below. However, the details of the kinetic expressions are skipped as it is out of the scope of this paper.

Drying and condensation reaction:
$H2O_{(l)} \leftrightarrow H2O_{(g)}$
The wet sinter bed is dried by the flow of hot flue gases from the coke combustion. The moisture in flue gas condensates as it cools at the lower part of the bed. The drying/condensation rate R_{H2O} (mol/(m³·s)) depends on the saturation pressure of the warm air $p_{sat}(T_s)$ and the partial pressure of the water vapour p_{H2O}, etc.

Coke burnout:
$C_{(s)} + O2_{(g)} \rightarrow CO2_{(g)}$
The coke in the raw mix reacts with the oxygen in the sucked air after the ignition zone. This reaction supplies the heat energy to the sintering process. The temperature of the raw mix is increased up to the melting point and it partially melts and solidifies in the form of a porous sinter cake. The reaction rate is obtained by multiplying r_C (mol/s) with number of coke particles per unit volume N_C (1/m³).

Calcination reaction:
$CaCO3_{(s)} \rightarrow CaO_{(s)} + CO2_{(g)}$
A main component of the sinter mix material is limestone (it is seen as CaCO3 in the model). The thermal decomposition of limestone occurs at temperatures of about 600°C and is an endothermic process. The reaction rate is obtained by multiplying r_{Ca} (mol/s) with number of limestone particles per unit volume N_L (1/m³).

Sulfation reaction:
$CaO_{(s)} + SO2_{(g)} + \frac{1}{2} O2_{(g)} \leftrightarrow CaSO4_{(s)})$
The reaction rate of calcium sulphate is obtained by multiplying r_S (mol/s) with number of lime particles per unit volume N_L (1/m³). Sulphur is introduced into the sinter mix with the coke combustion. The sulphur generation rate is set $f_S^{coke} = 0.01$ times the coke burn-out reaction rate. Since the measurements in laboratory and operational trials showed no significant influence on the SO2-emissions, this aspect was not further focused during the model development.

Total mass and energy balances:
Additionally, many process relevant quantities are computed by using the global ordinary differential equations (ODEs) feature in the COMSOL®. These quantities are: total gas volume, total energy inlet, total energy outlet, total energy inlet at ignition hood, total inlet substances and total outlet substances with X=(N2, O2, CO2, SO2, H2O).

Main Simulation Results

The ignition of the coke in the mix bed is usually performed by using combustion gas, which heats the inlet air to approximately 1200°C. The inlet air temperature and ignition energy as well as the suction pressure are summarized in Figure 8. Note that the pressure is scaled by 10 for better visibility.

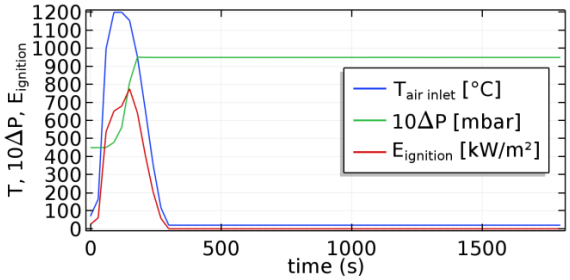

Figure 8. The inlet air temperature and ignition energy as well as the suction pressure.

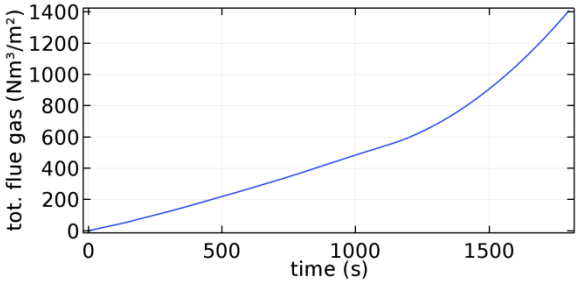

Figure 9. Total flue gas volume (Nm³/m²-bed)

The total flue gas volume as Norm-m³/m²-bed as shown in Figure 9 is also a direct output of the model. This curve is very closely related to the suction pressure and the flue gas fan curve as well as burn-through-point (BTP) and the sinter bed speed. The BTP indicates the completing of the sintering process. Therefore, the sinter bed speed is regulated in such a way that the BTP happens shortly before the discharge.

To understand the energy flow in the sintering process, the specific energies given to the sinter bed by air, coke, drying, and lime decomposition should be analyzed. The main energy supply is the coke in the mix bed as shown in Figure 10. Additionally,

some contribution comes from the hot gas during the ignition. Some of the energy is utilized to decompose the limestone and dry the moisture in the mix bed. In practice, very little energy is released into exhaust gas since the heat in the flue gas heats the mix bed at lower layers. Once all the mix bed is sintered, then the flue gas temperatures clearly raises, indicating the BTP and process completion.

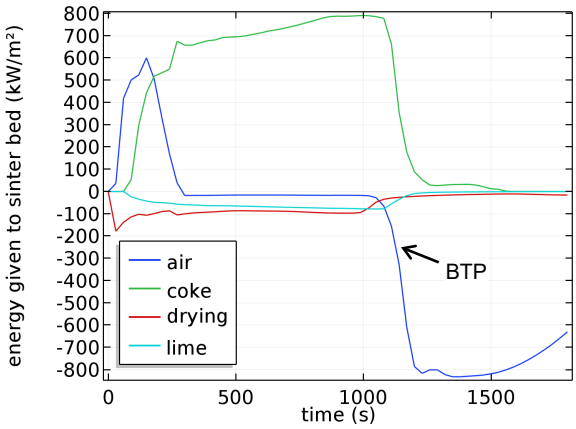

Figure 10. Specific energies given to the sinter bed.

Figure 11 compares the thermal profiles taken at the discharge with the calculated bed temperature profile at t=1200s. Two horizontal rows of permeability bars are used. A rather simple camera was used to record the thermal profile which allows distinguishing only the glowing areas and cold areas which fit quite good to the simulation of ideal process states.

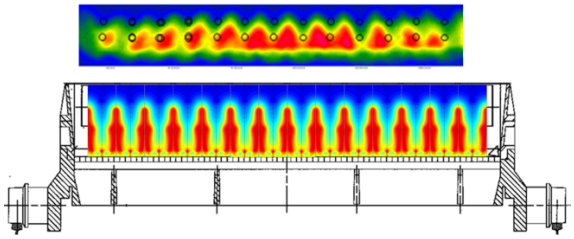

Figure 11. Simulated and measured high temperature zone at discharge (two rows of horizontal bars with 200mm horizontal spacing).

The focus of this study is to use the sintering process model to improve the efficiency by optimizing the permeability bar configurations. To exhibit the model capabilities, two different configurations and their influence on the bed temperature, coke burn-out, and drying during the progress of the process are compared on the next page (i.e. from Figure 12 up to Figure 19).

If the temperature profiles in Figure 13 and Figure 17 are carefully observed, one can see how the sinter process is accelerated in the permeability bar region as compared to neighboring unaffected base bed. In consistency with industrial results, the process speed can be increased by up to approximately 40% according to the simulation results.

In Figure 14 and Figure 18, the remaining coke fraction is defined by the ratio of the remained mass of the coke per unit volume to its initials value.

Prior to the use of permeability bars, the high quality differences between the topmost and the lowest regions of the bed have been investigated by many researchers. A good correlation between the area below the time-temperature curve for temperatures above 1200°C and the sinter cold strength have been observed. So far, the sinter process models are just focused on the vertical differences which are inherent to the system since the lower areas profit from the heat which is brought in by the hot process gas from above.

The most obvious influence is remarkable on the temperature field, which has a direct effect on the sinter quality. Hence, a sinter quality estimation model has been also implemented which uses the area below the time-temperature curve above 1200°C to estimate the cold strength of the sinter produced:

$$ITT_{1200} = \int_0^t \text{if}(T_s > 1200°C, T_s - 1200°C, 0)dt$$

The time-temperature curves for four representative points are shown in Figure 20. The temperatures at point 3 and point 4 (strongly aerated area and below) barely exceed 1200°C hence poorer sinter quality (strength) is expected at these two points whereas at positions 1 and 2 a better sinter quality is expected due to a long duration at high temperature.

The new model thus provides a completely new understanding of the actual local process conditions. The information about the local time-temperature curves can be exploited to estimate the local cold strength, which is of prime importance in assessing the sinter quality. The most common testing methods for assessing the strength of cold sinter may be grouped into three categories: drop or shatter test, impact test, and tumble test or abrasion test. For example, the quality can be defined as the percentage of sinter material having size larger than 6.3mm after a characteristic tumbling procedure. The interpolation function given in Table 2 can be used for estimation of the quality according to this definition.

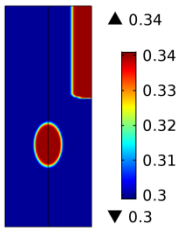

Figure 12. Porosity distributions for one row of horizontal and vertical permeability bars.

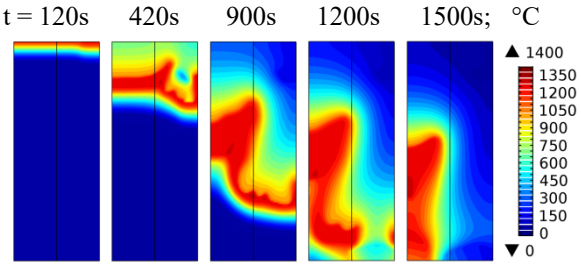

Figure 13. Temperature evolution for the bar configuration shown in Figure 12.

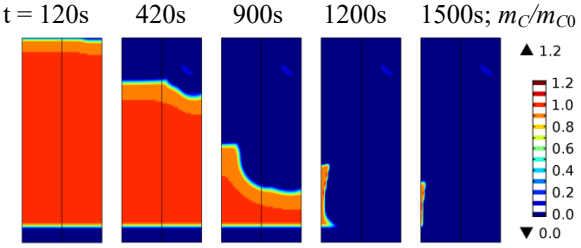

Figure 14. Remaining coke fraction for the bar configuration shown in Figure 12.

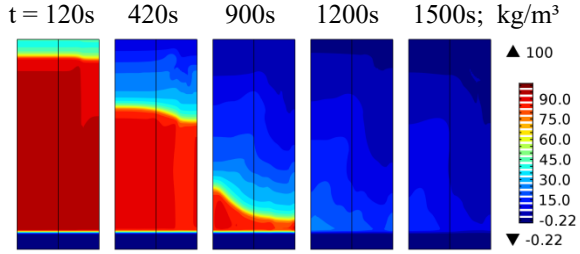

Figure 15. Moisture content for the bar configuration shown in Figure 12.

The estimated local sinter strength distributions for the permeability bar configurations of Figure 12 and Figure 16 are compared in Figure 21 for the process state some minutes before the discharge. Note that the regions having quality less than 50% in the lower areas are kept empty. Here the sinter process is not yet finished.

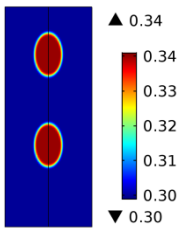

Figure 16. Porosity distributions for two rows of horizontal permeability bars.

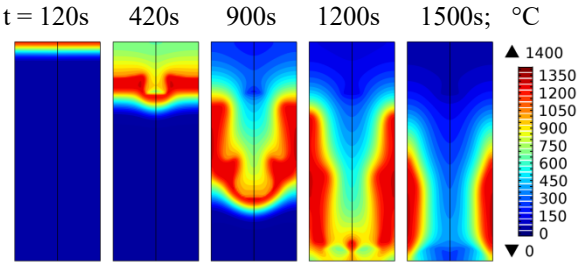

Figure 17. Temperature evolution for the bar configuration shown in Figure 16.

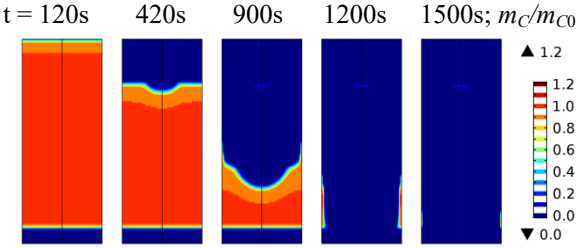

Figure 18. Remaining coke fraction for the bar configuration shown in Figure 16.

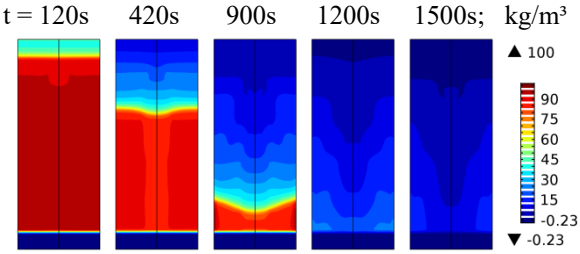

Figure 19. Moisture content for the bar configuration shown in Figure 16.

The model results obtained for different permeability bar configurations were verified with industrial trials and measurements. Both of the verifications showed consistently that the sinter speed can be raised up to as high as 40% with a well-adjusted permeability bar configuration. Inevitably the average sinter strength decreases slightly as the local inhomogeneities are raised even for well-adjusted permeability bars.

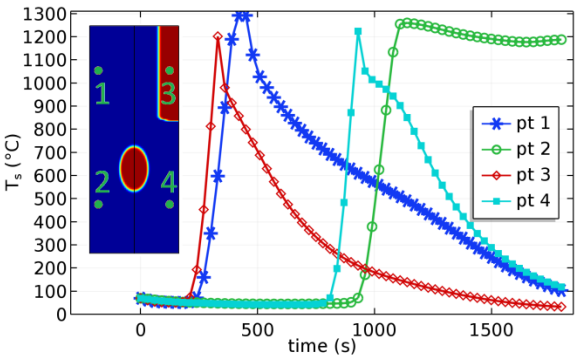

Figure 20. Time-temperature curves.

Table 2: ITT_{1200} and quality relation

ITT_{1200} (K· s)	$\log_{10}(ITT_{1200})$	Cold strength
100 [K · s]	2	50 [%]
5 000 [K · s]	3.70	78 [%]
12 000 [K · s]	4.08	91 [%]
35 000 [K · s]	4.54	93 [%]
100 000 [K · s]	5	95 [%]

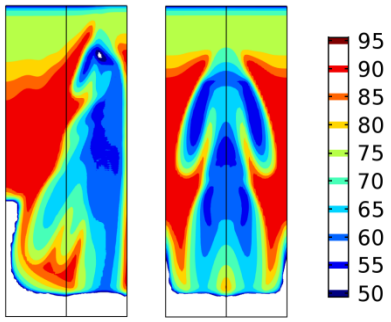

Figure 21. Quality estimations for permeability bar configurations as in Figure 12 (left side) and as in Figure 16 (right side).

Conclusions

The modification of the local flow through the sinter mix bed induced by local aeration is the booster of a bunch of complex spatial consequences on the sinter process (temperature, combustion front, calcination and drying progress). The heterogeneity of the flow field not only initializes local heterogeneity of the sinter process progress but also dominates the local convective heat supply.

The permeability bars were proven to raise the cold permeability to some extent but the folding of the burn-through profile across the strand width is even more effective. The bars raise the cold permeability just locally within a few centimeters scope from the bars. The local scopes are similar even for very different sinter mixes. The influences of horizontal and vertical permeability bars interact and may cause detrimental effects unless properly tuned. The sinter process speed (productivity) can be raised by up to 40% with optimum permeability bar configuration. Since even properly designed bars increase the local inhomogeneities, the average sinter strength usually decreases slightly.

Optimum results were obtained either with two stacked rows of horizontal bars with approximately 20cm spacing or with a combination of vertical bars with 30-40cm spacing and horizontal bars in-between. The bar design can be further optimized basing on a statistic analysis of the thermal profiles at discharge supported by calculations with the new 2D sinter process model.

The results of the model provide a change of paradigm in sinter process simulation since they prove that the lateral differences cannot be neglected any more. As future work, the model can be extended to include the influence of the diffusion and the dispersion phenomena in the convection equations. Moreover, a sub-model for the NOx emission can be implemented. Furthermore, the estimation of the sinter quality, the set of the chemical reactions and the involved species can be extended to increase model accuracy and capabilities. Implementation of a user friendly app-interface for the plant operators would be also worthy.

References

1. T. Hauck, *et. al.*, *Optimisation of permeability bars to customise sinter plants on changing demands*, 1-146, European Commission, Luxemburg (2017)
2. F. Cappel, *Sintern von Eisenerzen*, 1-293, Verlag Stahleisen M.B.H., Düsseldorf (1973)

Acknowledgements

The work presented here has been carried out with a financial grant from the Research Fund for Coal and Steel (RFCS) of the European Community with Grant Agreement No: RFSR-CT-2011-00004 and project title *"Optimisation of permeability bars to customise sinter plants on changing demands" (OPTIPER)*.

Furthermore, the authors greatly acknowledge the support from the company "Thyssenkrupp Steel Europe AG" and especially Mr. Lischke and his colleagues, which organized the in-situ test. In addition, the authors gratefully acknowledge the intensive cooperation among the other project partners and authors colleges Mr. Hauke Bartusch and Mr. Stefan Böhnisch.